Acta Geochim (2021) 40(5):702–717
https://doi.org/10.1007/s11631-021-00485-z

ORIGINAL ARTICLE

Late Jurassic adakitic ore-bearing granodiorite porphyry intrusions in the Xiaokele porphyry Cu (–Mo) deposit, Northeast China: implications for petrogenesis and tectonic setting

Yonggang Sun[1,2] · Bile Li[1] · Zhonghai Zhao[2] · Qingfeng Ding[1] · Fanbo Meng[3] · Xusheng Chen[3] · Ye Qian[1,4] · Yujin Li[1,4]

Received: 18 April 2021 / Revised: 9 June 2021 / Accepted: 10 June 2021 / Published online: 28 June 2021

Abstract The Xiaokele Cu (–Mo) deposit is a recently discovered porphyry deposit in the northern Great Xing'an Range (GXR) of northeast China. The ore bodies in this deposit are mainly hosted within granodiorite porphyry intrusions. Potassic, phyllic, and propylitic alteration zones develop from center to edge. In this paper, we present zircon LA–ICP–MS U–Pb ages, zircon Hf isotopic compositions, and whole-rock geochemistry of the ore-bearing granodiorite porphyries from the Xiaokele Cu (–Mo) deposit. Zircon U–Pb dating suggests that the Xiaokele granodiorite porphyries were emplaced at 148.8 ± 1.1 Ma (weighted-mean age; n = 14). The Xiaokele granodiorite porphyries display high SiO_2, Al_2O_3, Sr, and Sr/Y, low K_2O/Na_2O, MgO, Yb, and Y, belonging to high-SiO_2 adakites produced by partial melting of the subducted oceanic slab. Marine sediments were involved in the magma source of the Xiaokele granodiorite porphyries, as indicated by enriched Sr–Nd isotopic compositions ($\varepsilon_{Nd}(t)$ = − 1.17– − 0.27), low positive zircon $\varepsilon_{Hf}(t)$ values (0.4–2.2), and high Th contents (4.06–5.20). The adakitic magma subsequently interacted with the mantle peridotites during ascent through the mantle wedge. The Xiaokele granodiorite porphyries were derived from slab melting during the southward subduction of the Mongol–Okhotsk Ocean.

Keywords Xiaokele porphyry Cu (–Mo) deposit · Adakite · Slab melting · Mongol–Okhotsk Ocean · Northern Great Xing'an Range

1 Introduction

Porphyry deposits are the main source of Cu, accounting for about 80% of the world's Cu reserves (Sillitoe 2010; Sun et al. 2015). Generally, most porphyry deposits occur in island arc and continental margin arc settings (Sillitoe 2010; Richards 2011a). Recently, discoveries of some world-class porphyry Cu (Mo–Au) deposits in some continental collision orogens (e.g., Qinling–Dabie Orogen)

✉ Bile Li
libl@jlu.edu.cn

Yonggang Sun
xg429805791@163.com

Zhonghai Zhao
zhaozhonghai_99@163.com

Qingfeng Ding
dingqf@jlu.edu.cn

Fanbo Meng
104445056@qq.com

Xusheng Chen
2399866894@qq.com

Ye Qian
qianye@jlu.edu.cn

Yujin Li
28004036@qq.com

[1] College of Earth Sciences, Jilin University, 2199 Jianshe Street, Changchun 130061, China

[2] College of Mining, Liaoning Technical University, Fuxin 123000, China

[3] Qiqihaer Institute of Geological Exploration, Heilongjiang 161006, China

[4] Key Laboratory of Mineral Resources Evaluation in Northeast Asia, Ministry of Land and Resources, Changchun 130061, China

indicate they may also form in post-subduction collisional settings (Chen and Santosh 2014; Richards 2015; Chen et al. 2017a). Porphyry Cu deposits are generally closely correlated with intermediate-felsic porphyritic intrusions with high oxygen fugacity (Mungall 2002; Shen et al. 2015; Zhang et al. 2017) and high water contents ($\geq$ 4 wt.%; Richards 2011b). Interestingly, most of these porphyries display the geochemical characteristics of adakites (e.g., $SiO_2 \geq 56$ wt.%; $Al_2O_3 \geq 15$ wt.%; $Y \leq 18$ ppm; $Yb \leq 1.9$ ppm; and $Sr \geq 400$ ppm; Defant and Drummond 1990; Sajona and Maury 1998; Oyarzu´n et al. 2001; Mungall 2002; Reich et al. 2003; Hollings et al. 2011; Sun et al. 2015).

Northeast (NE) China is located in the eastern part of the Central Asian Orogenic Belt (CAOB), adjacent to the Siberia Craton in the north and the Tarim-North China Craton in the south (Fig. 1A; Şengör et al. 1993; Jahn et al. 2004). The Great Xing'an Range (GXR) lies in the western part of NE China (Fig. 1B), is a vitally important polymetallic metallogenic belt in China (Song et al. 2015; Chen et al. 2017b). During previous decades, several epithermal and orogenic Au deposits, porphyry deposits, hydrothermal-vein Ag–Pb–Zn deposits, and skarn Pb–Zn deposits have already been discovered in the northern GXR (Fig. 1C). The Xiaokele porphyry Cu (–Mo) deposit, located in the northern GXR, was discovered by the Qiqihaer Institute of Geological Exploration in 2013. This deposit contains estimated reserves of > 500,000 tons Cu with grades of 0.2%–4.41%, > 100,000 tons Mo with grades of 0.03%–0.70%, and > 53 tons Ag, with ongoing exploration (Sun et al. 2020a). The discovery of this deposit is an important breakthrough for porphyry Cu prospecting in the northern GXR. The published whole-rock geochemical data for Late Jurassic ore-bearing granodiorite porphyries in the Xiaokele deposit exhibit adakitic affinity (Deng et al. 2019a; Feng et al. 2020a). However, two quite different genetic models for the adakitic ore-bearing granodiorite porphyries lead to difficulties in understanding their petrogenesis and Late Mesozoic tectonic evolution. Deng et al. (2019a) suggested that the Xiaokele granodiorite porphyries were formed by the partial melting of an altered oceanic slab associated with the southward subduction of the Mongol–Okhotsk oceanic slab, whereas Feng et al. (2020a) considered the Xiaokele granodiorite porphyries were derived from partial melting of an enriched mantle metasomatized by subduction-related melts in a post-collision setting.

To solve the above problem, in this study, we present zircon LA–ICP–MS U–Pb ages, zircon Hf isotopic compositions, and whole-rock geochemistry of the adakitic ore-bearing granodiorite porphyries from the Xiaokele Cu (–Mo) deposit. We discuss their petrogenesis and implications for tectonic settings.

Fig. 1 **A** Location of the Central Asian Orogenic Belt (Jahn et al. 2000). **B** Geological map of NE China (Chen et al. 2012). Fault abbreviations: F1, Mongol–Okhotsk; F2, Tayuan–Xiguitu; F3, Hegenshan–Heihe; F4, Mudanjiang–Yilan; F5, Solonker–Xar Moron–Changchun–Yanji; F6, Jiamusi–Yilan; F7, Dunhua–Mishan. **C** Geological map of the northern Great Xing'an Range (modified from Deng et al. 2019b), showing the distribution of major deposits

2 Geological background

From east to west, NE China is divided into the Jiamusi–Khanka, Songnen, Xing'an, and Erguna blocks (Fig. 1B; Wu et al. 2011). During the Paleozoic, these blocks collided and amalgamated, triggered by the subduction and closure of the Paleo-Asian Ocean (Şengör et al. 1993; Wu et al. 2011; Zhou et al. 2018). During the Mesozoic, NE China was not only influenced by the Paleo-Pacific tectonic regime but also superimposed and modified by the Mongol–Okhotsk tectonic regime (Wu et al. 2011; Xu et al. 2013; Liu et al. 2017).

The Xiaokele Cu (–Mo) deposit is situated in the eastern part of the Erguna Block (Fig. 1C). The Erguna Block lies between the Mongol–Okhotsk, and Tayuan–Xiguitu sutures (Fig. 1C). Studies on early Paleozoic blueschist facies metamorphic rocks and post-orogenic granites suggest that Xing'an and Erguna blocks collided along the Tayuan-Xiguitu suture at ca. 500 Ma (Fig. 1C; Ge et al. 2005; Zhou et al. 2015). The basement of the Erguna Block is mainly composed of Precambrian metamorphic supracrustal rocks and sporadic Paleoproterozoic and Neoproterozoic granitoids (Inner Mongolian Bureau of Geology and Mineral Resources (IMBGMR) 1991; Miao et al. 2004; Zhou et al. 2011). Outcropping strata are mainly Paleozoic shallow marine sediments (IMBGMR 1996), widespread Mesozoic volcanic rocks, and minor Cenozoic terrigenous clastic rocks (Zhang et al. 2008). Late Mesozoic NE-trending Derbugan and Erguna River faults develop in the Erguna Block (Fig. 1C; IMBGMR 1991). Intrusive rocks (granitic rocks are predominant) in the Erguna Block were mainly emplaced during Paleozoic and Mesozoic (Fig. 1C; Wu et al. 2011; Gou et al. 2017).

3 Deposit geology

3.1 Ore district geology

The Xiaokele porphyry Cu (–Mo) deposit is located ~ 20 km north of Tayuan Town in Heilongjiang Province (Fig. 1C). From old to young, the outcropping strata in this area are mainly the Neoproterozoic–Lower Cambrian

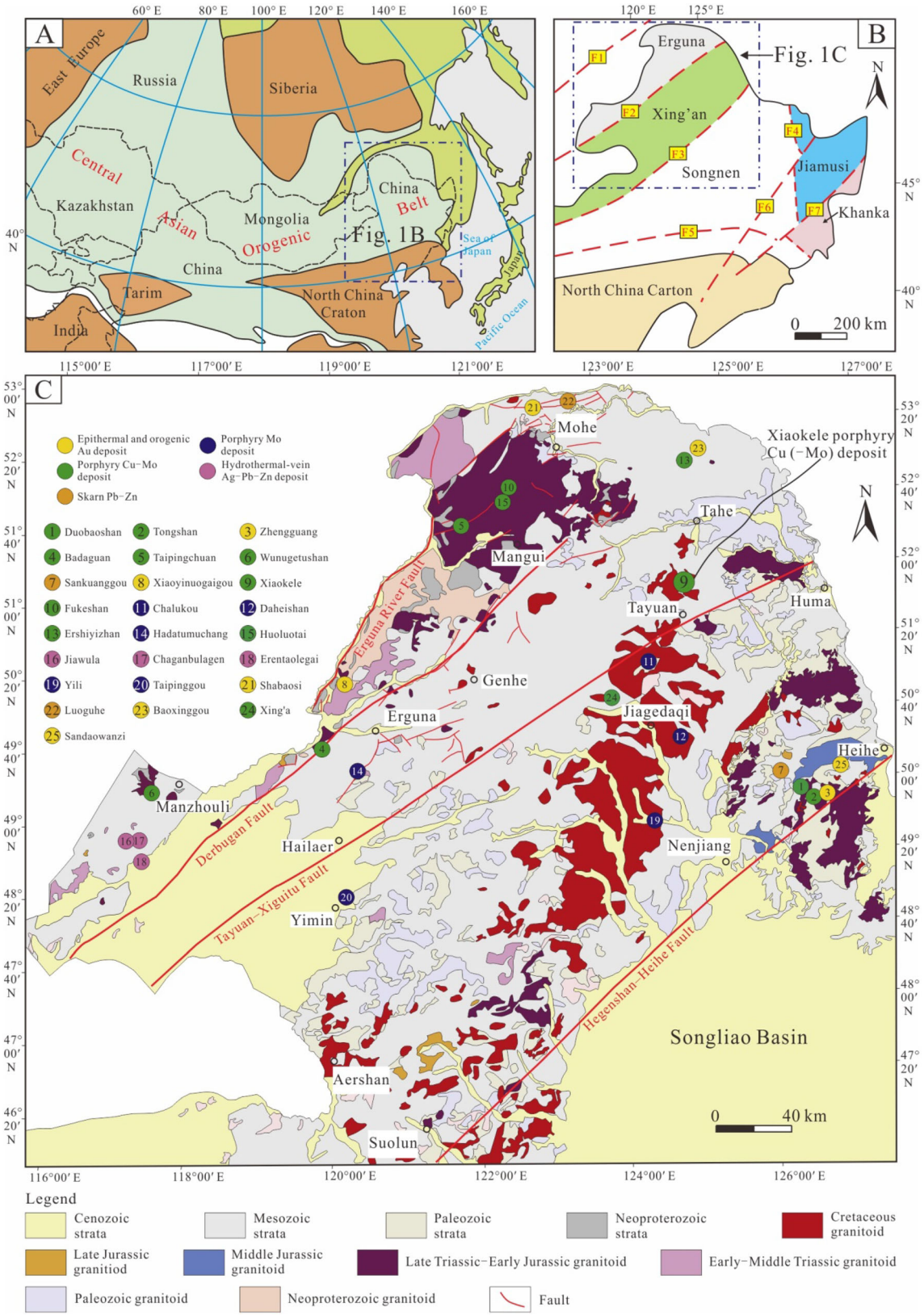
A
East Europe
Russia
Siberia
Central
Kazakhstan
Asian
Orogenic
Mongolia
China
Belt
Fig. 1B
Sea of Japan
Japan
Tarim
India
North China Craton
Pacific Ocean
B
Erguna
Fig. 1C
Xing'an
Songnen
Jiamusi
Khanka
North China Carton
F1
F2
F3
F4
F5
F6
F7
0 200 km
C
Epithermal and orogenic Au deposit
Porphyry Cu–Mo deposit
Skarn Pb–Zn
Porphyry Mo deposit
Hydrothermal-vein Ag–Pb–Zn deposit
1 Duobaoshan
2 Tongshan
3 Zhengguang
4 Badaguan
5 Taipingchuan
6 Wunugetushan
7 Sankuanggou
8 Xiaoyinuogaigou
9 Xiaokele
10 Fukeshan
11 Chalukou
12 Daheishan
13 Ershiyizhan
14 Hadatumuchang
15 Huoluotai
16 Jiawula
17 Chaganbulagen
18 Erentaolegai
19 Yili
20 Taipinggou
21 Shabaosi
22 Luoguhe
23 Baoxinggou
24 Xing'a
25 Sandaowanzi
Mohe
Xiaokele porphyry Cu (−Mo) deposit
Tahe
Mangui
Tayuan
Huma
Erguna River Fault
Genhe
Erguna
Jiagedaqi
Heihe
Manzhouli
Derbugan Fault
Hailaer
Nenjiang
Tayuan–Xiguitu Fault
Yimin
Hegenshan–Heihe Fault
Songliao Basin
Aershan
Suolun
0 40 km
Legend
Cenozoic strata
Mesozoic strata
Paleozoic strata
Neoproterozoic strata
Cretaceous granitoid
Late Jurassic granitiod
Middle Jurassic granitoid
Late Triassic–Early Jurassic granitoid
Early–Middle Triassic granitoid
Paleozoic granitoid
Neoproterozoic granitoid
Fault

Jixianggou and Dawangzi Formations, Upper Jurassic Baiyingaolao Formation, and Quaternary sediments (Fig. 2A). The Jixianggou Formation is mainly composed of phyllite, schist, marble, slate, feldspar-bearing quartz siltstone, and metamorphic sandstone. The Dawangzi Formation is mainly composed of metamorphosed intermediate–basic lava interbedded with metamorphosed acidic lava and slate. The main rocks in the Baiyingaolao Formation are rhyolitic tuff and rhyolite, which rests unconformably on the Dawangzi and Jixianggou Formations. The Xiaokele Cu (–Mo) deposit is located near the junction of the NNW–trending Dawusu River and NEE–trending Xiaokele River faults (Fig. 2A). Multiphase intrusive rocks are developed in the Xiaokele mining area, including the early Permian syengranite (292.5 ± 0.9 Ma, Sun et al. 2020b), Late Jurassic granodiorite porphyry (150.0 ± 1.6 Ma), and diorite porphyrite (147.9 ± 1.3 Ma), and Early Cretaceous granite porphyry (123.2 ± 1.7 Ma) (Deng et al. 2019a). The granodiorite porphyry, whose outcrop area is ~ 1.6 km^2 (Fig. 2A), is considered as the ore-bearing rocks and is closely related to the associated hydrothermal alteration of this deposit. The granodiorite porphyry is gray-white and exhibits porphyritic texture, it consists of 65%–70% phenocrysts and 30%–35% fine-grained groundmass (Fig. 3A, B). Phenocrysts are dominantly composed of quartz (25%–30%), plagioclase (25%–30%), alkali-feldspar (5%–10%; including perthite and orthoclase), biotite (~ 5%), and hornblende (< 5%), with minor accessory sphene (1%–2%) (Fig. 3C), the groundmass has the same composition as the phenocrysts.

3.2 Alteration and mineralization

Based on drilling, mineralization is mainly located at the top and center part of the granodiorite porphyry in the Xiaokele porphyry Cu (–Mo) deposit (Fig. 2B). The orebodies are generally 100–1050 m long and 4–112 m thick (Fig. 2B). Three alteration zones can be divided, from center to edge, into potassic, phyllic, and propylitic alteration zones (Fig. 2B). The potassic alteration zone is mainly distributed in the center of the granodiorite porphyry (Fig. 2B), and potassic alteration is characterized by secondary biotite and K-feldspar (Fig. 3D). The potassic alteration zone mainly contains magnetite, hematite, chalcopyrite, and molybdenite (Fig. 3D–F). Phyllic alteration is characterized by secondary quartz and sericite (Fig. 3G, H). Phyllic alteration overprinted the preexisting potassic alteration. Pyrite, chalcopyrite, and molybdenite are developed in the phyllic alteration zone (Fig. 3G, H). The

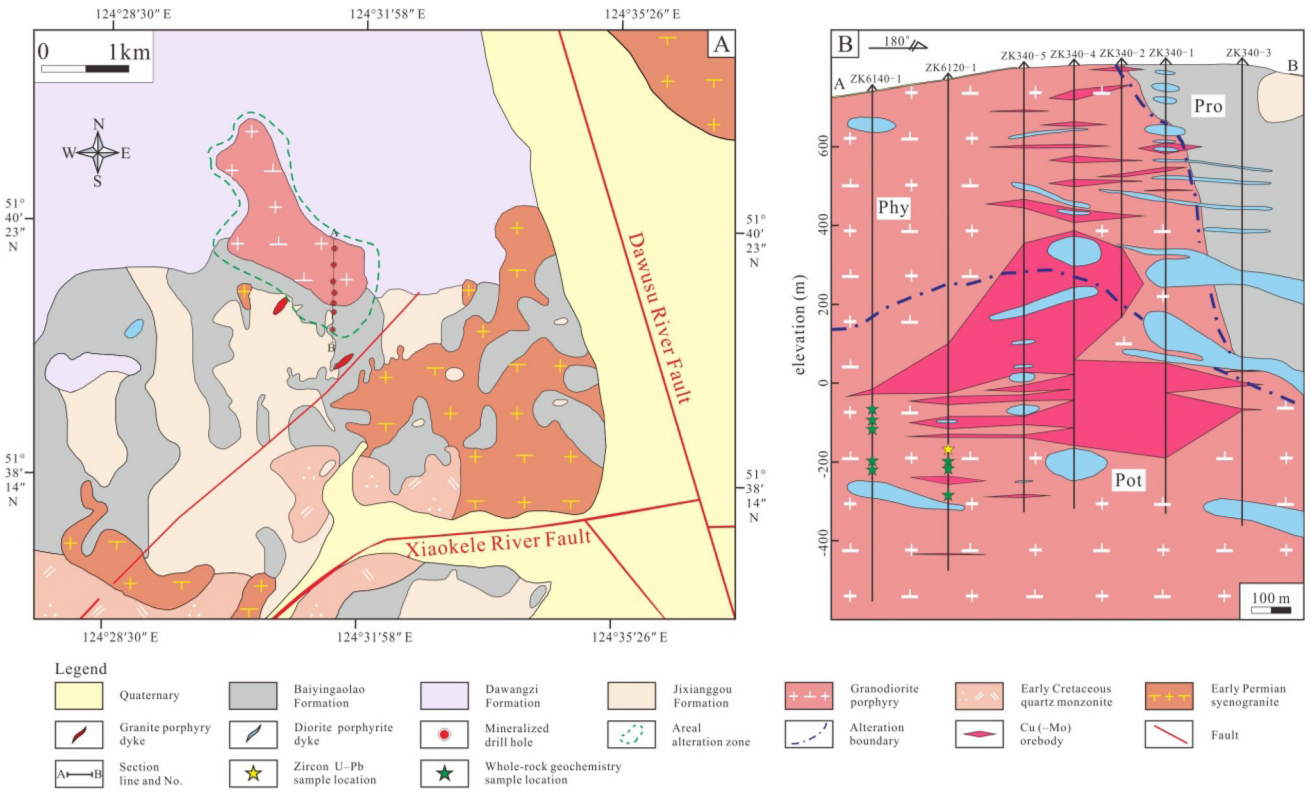

Fig. 2 **A** Geological map of the Xiaokele Cu (–Mo) deposit (modified from Qiqihaer Institute of Geological Exploration (QIGE 2018). **B** Geological sections along the **A**–**B** exploration lines of the Xiaokele Cu (–Mo) deposit with sample locations as indicated (modified from QIGE, 2018). Abbreviations: Pot = potassic alteration zone; Phy = phyllic alteration zone; Pro = propylitic alteration zone.

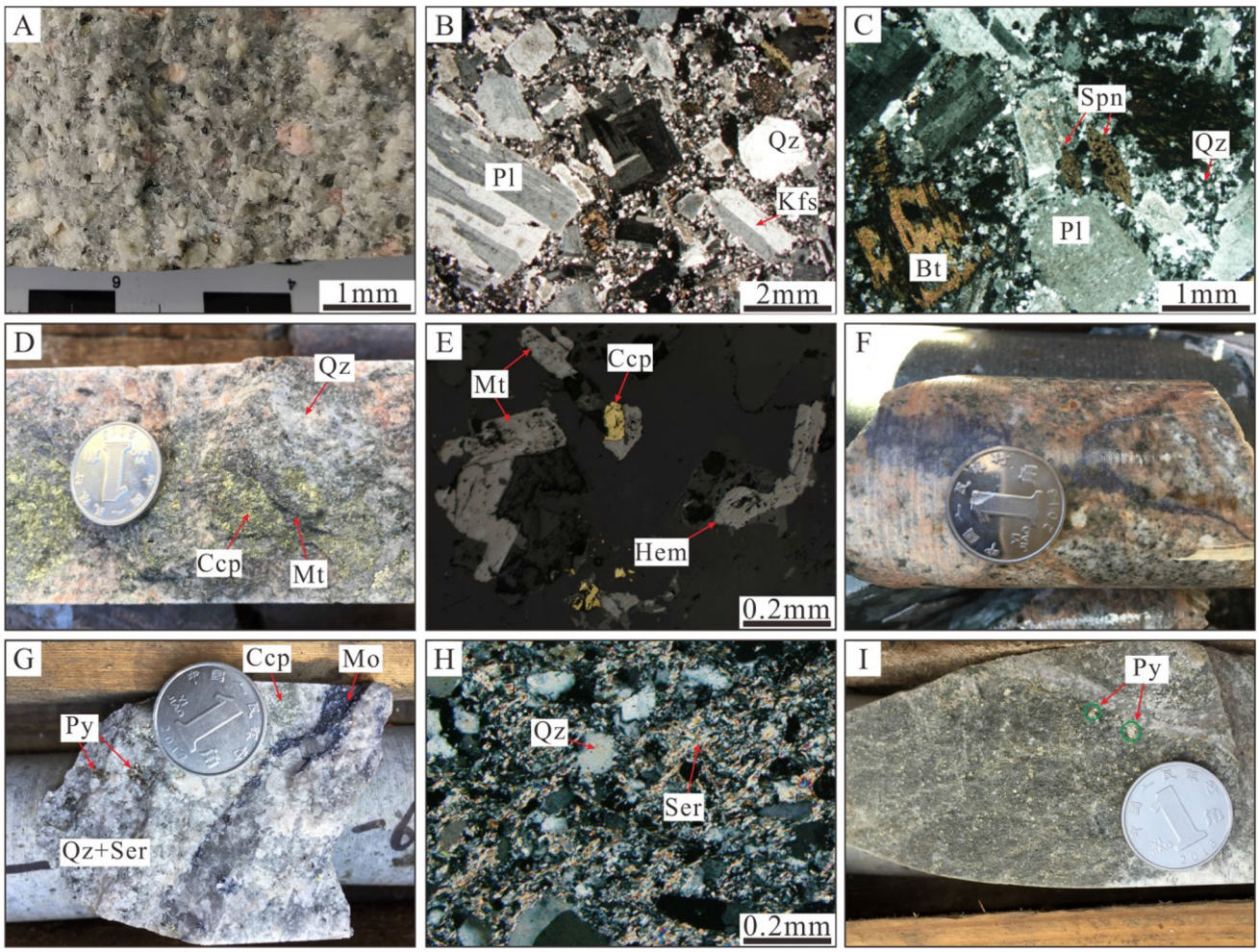

Fig. 3 Photographs and photomicrographs of granodiorite porphyry and representative hydrothermal alteration features in the Xiaokele Cu (–Mo) deposit. **A** Hand specimen of granodiorite porphyry. **B–C**) Photomicrographs of granodiorite porphyry. **D** Quartz + magnetite + chalcopyrite assemblage in potassic-altered granodiorite porphyry. **E** Magnetite, hematite, and minor chalcopyrite in the potassic-altered wall rock. **F** Quartz + molybdenite vein with K-feldspar alteration halos. **G** Disseminated molybdenite, chalcopyrite, and pyrite associated with intensive phyllic alteration. **H** Phyllic alteration, with the alteration assemblage of quartz and sericite. **I** Propylitic alteration with minor disseminated pyrite in granodiorite porphyry. Abbreviations: Qz = quartz; Kfs = K-feldspar; Bt = biotite; Pl = plagioclase; Spn = sphene; Ep = epidote; Ser = sericite; Hem = hematite; Mt = magnetite; Py = pyrite; Ccp = chalcopyrite; Mo = molybdenite

propylitic alteration zone forms at the periphery of the deposit. It is characterized by chlorite, epidote, and calcite, with minor disseminated pyrite (Fig. 3I). Most Cu–Mo mineralization occurs in the middle-upper part of the potassic alteration zone and the lower part of the phyllic alteration zone (Fig. 2B).

4 Analytical methods

4.1 Zircon U–Pb dating

Zircon crystals were separated from the granodiorite porphyry samples using standard heavy liquid and magnetic techniques, and then the zircon crystals were handpicked under a binocular microscope at the Shangyi Geologic Service, Langfang, China. All zircon crystals were examined by Cathode Luminescence (CL) imaging to reveal their internal structures. Laser ablation inductively coupled mass spectrometry (LA–ICP–MS) zircon U–Pb dating and trace element analyses were undertaken at Yanduzhongshi Geological Analysis Laboratories, Beijing. The laser ablation system is New Wave UP213 and ICP-MS is Aurora M90. Analyses were carried out with a beam diameter of 30 μm, ablation rate of 10 Hz, and energy density of 2.5 J/cm^2. Detailed experimental testing procedures were described by Yuan et al. (2004). Helium was used as the carrier gas, and argon was used as compensation gas. Zircon 91,500 was used as the external standard for U–Pb dating. Trace element compositions of zircon

crystals were quantified using SRM610 as an external standard, and Si was used as an internal standard (Liu et al. 2010a). Correction of common Pb was evaluated using the method described by Andersen (2002). The ICP–MS DATECAL program was used to calculate isotopic data and elemental contents (Liu et al. 2008). Isoplot/Ex_ver3 was used to perform age calculations and generate Concordia diagrams (Ludwig 2003). The uncertainties for individual analyses are quoted at the 1σ confidence level. Zircon U–Pb dating and zircon trace element composition data are presented in Table S1 and Table S2, respectively.

4.2 Whole-rock major and trace element analyses

Eight granodiorite porphyry samples were sampled distal to the location of mineralization and alteration. The freshest parts of the samples without alteration were selected for whole-rock geochemistry analysis before being crushed to 200 mesh. All whole-rock geochemistry analyses were conducted at the Key Laboratory of Mineral Resources Evaluation in Northeast Asia, Ministry of Land and Resources, Jilin University, Changchun, China. Major element compositions were determined by X-ray fluorescence (XRF) spectroscopy and fused glass disks. Trace element compositions were determined by an Agilent 7500a ICP–MS after the sample powders were dissolved in HF in Teflon bombs. The analytical precision was better than 5% for major elements, and was better than 10% for trace elements, as estimated by using the international standards BHVO-2 and BCR-2, and national standards GBW07103 and GBW07104. The analytical results of major and trace elements are listed in Table S3.

4.3 Zircon Hf isotopic analyses

Zircon Lu–Hf isotope analysis was carried out in-situ by using an NWR193 laser-ablation microprobe (Elemental Scientific Lasers LLC), attached to a Neptune multicollector ICP-MS at Yanduzhongshi Geological Analysis Laboratories, Beijing, China. The ablation spots for the Hf isotope analyses were located over the positions on the zircon crystals previously analyzed for zircon U–Pb dating. We adopted a beam diameter of 40 μm, ablation time of 31 s, ablation rate of 8 Hz, and energy density of 16 J/cm^2. Detailed instrumental conditions, analytical procedures, and data acquisition techniques were comprehensively described by Wu et al. (2006). Zircon 91,500 and Plesovice were used as the reference standards during our routine analyses. Hf isotopic composition data are listed in Table S4.

5 Analytical results

5.1 Zircon U–Pb ages and geochemistry

Zircons from the granodiorite porphyry samples are generally columnar (Fig. 4A). All analyzed zircons were euhedral to subhedral. Their oscillatory growth zoning, the Th/U ratios (0.80–1.30), and pronounced positive Ce anomalies (Fig. 4B) indicate a magmatic origin (Hoskin 2005). Fourteen zircons yielded $^{206}Pb/^{238}U$ ages of 152–145 Ma and a weighted-mean age of 148.8 ± 1.1 Ma (MSWD = 1.12; n = 14) (Fig. 4C, D). These results indicate that the granodiorite porphyry formed during Late Jurassic.

5.2 Whole-rock major and trace element compositions

The eight analyzed granodiorite porphyry samples display relatively high SiO_2 (63.01–65.70 wt.%), Al_2O_3 (15.83–16.43 wt.%), K_2O (2.79–3.32 wt.%), and Na_2O (4.90–5.54 wt.%), and low TiO_2 (0.54–0.73 wt.%), and MgO (1.18–1.36 wt.%). The granodiorite porphyry samples belong to the high-K calc-alkaline series (Fig. 5A). A/CNK ratios of 0.82–0.94 display metaluminous characteristics (Fig. 5B), with geochemical compositions similar to the published Late Jurassic-Early Cretaceous subducting oceanic crust-derived adakitic rocks in the northern GXR (Fig. 5; Deng et al. 2019a, b; Xu et al. 2020).

The chondrite-normalized REE patterns of all the granodiorite porphyry samples are slightly enriched in light rare-earth elements (LREEs) with respect to heavy rare-earth elements (HREEs) and show weak negative Eu anomalies ($Eu/Eu^* = 0.80–0.91$) (Fig. 6A). In the primitive mantle-normalized spider diagram (Fig. 6B), the granodiorite porphyry samples are depleted in Nb, Ta, and Ti and enriched in Rb, Ba, and K. These geochemical compositions are also in accordance with the published Late Jurassic-Early Cretaceous subducting oceanic crust-derived adakitic rocks in the northern GXR (Fig. 6; Deng et al. 2019a, b; Xu et al. 2020).

5.3 Zircon Hf isotopic compositions

Fourteen magmatic zircons from the granodiorite porphyry samples were analyzed for Lu–Hf isotopes, yielding initial $^{176}Hf/^{177}Hf$ ratios of 0.282692–0.282744 and positive $\varepsilon_{Hf}(t)$ values of 0.4–2.2 (Fig. 7), with corresponding T_{DM1} and T_{DM2} ages of 786–708 Ma and 1045–942 Ma, respectively (Table S4). The $\varepsilon_{Hf}(t)$ values plot in the field between the depleted mantle line and the chondrite evolution line (Fig. 7), similar to $\varepsilon_{Hf}(t)$ values of the

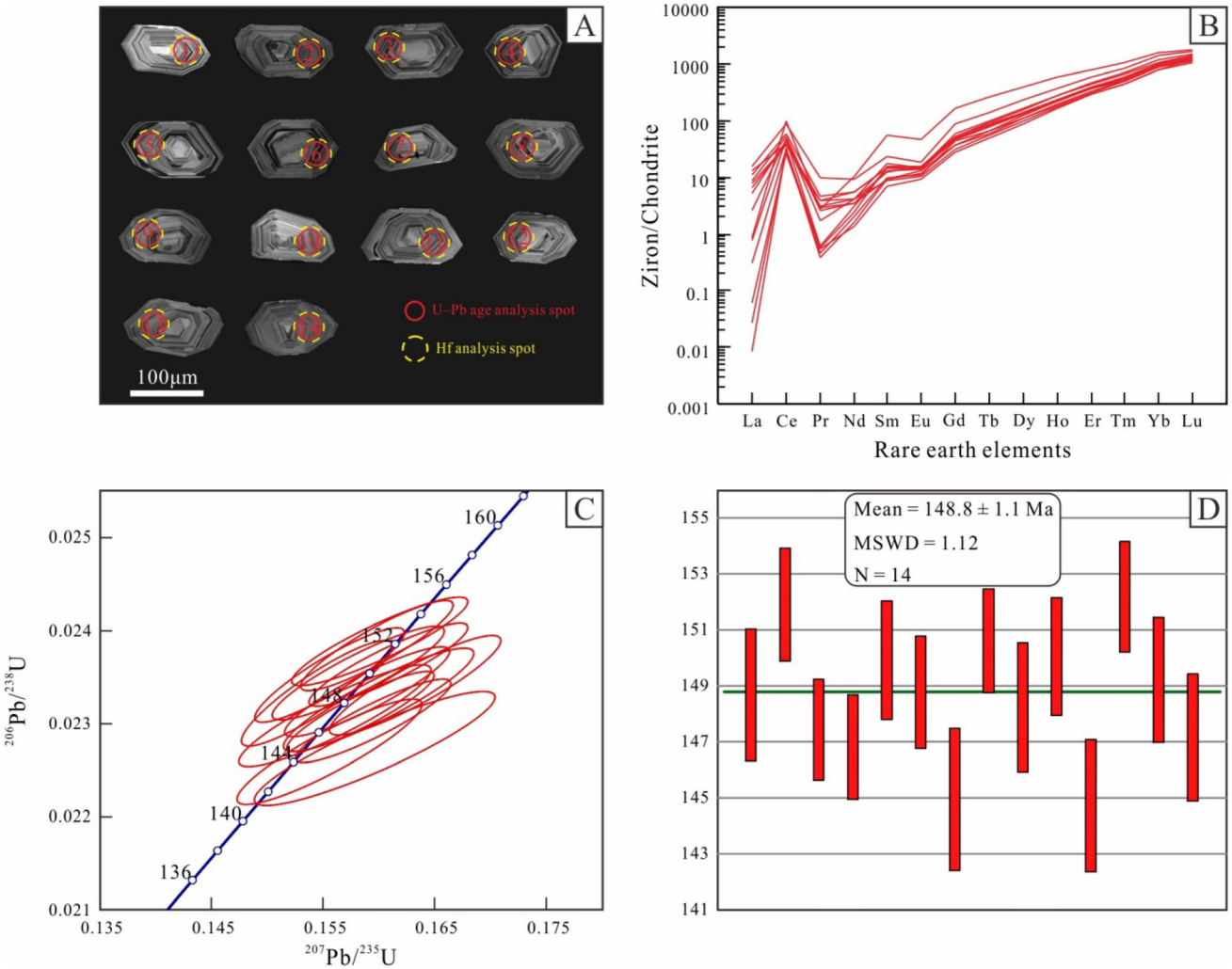

Fig. 4 **A** Cathode luminescence microphotographs of zircons for the granodiorite porphyry from the Xiaokele deposit. **B** Chondrite-normalized REE pattern of zircons for the granodiorite porphyry. The chondrite values are from Boynton (1984). **C**, **D** Zircon U–Pb Concordia diagram and weighted mean $^{206}Pb/^{238}U$ ages for the granodiorite porphyry from the Xiaokele deposit

Phanerozoic magmatic rocks in the east CAOB (Fig. 7A; Yang et al. 2006).

6 Discussion

6.1 Age of magmatism and mineralization

Deng et al. (2019a) showed that the zircon U–Pb ages of rhyolite, granodiorite porphyry, diorite porphyrite, and granite porphyry associated with the Xiaokele Cu (–Mo) deposit are 152.5 ± 1.7, 150.0 ± 1.6, 147.9 ± 1.3, and 123.2 ± 1.7 Ma, respectively. This evidence indicates that the granodiorite porphyry was emplaced after the rhyolite but before the granite porphyry and diorite porphyrite. Observations of the intrusive relationships between magmatic rocks also support this conclusion. The granodiorite porphyry intruded into the Baiyingaolao Formation rhyolite/rhyolitic tuff and was subsequently intruded by the granite porphyry and diorite porphyrite dykes (Fig. 2A, B).

In this study, the Xiaokele granodiorite porphyry yielded a weighted-mean age of 148.8 ± 1.1 Ma (Fig. 4D), which coincides well with molybdenite Re-Os isochron age (148.5 ± 1.5 Ma; Feng et al. 2020a, b). In addition, Cu (–Mo) mineralization is mainly hosted within granodiorite porphyry (Fig. 2B). Based on the evidence, we conclude that the Late Jurassic granodiorite porphyry most likely caused porphyry Cu (–Mo) mineralization in the Xiaokele Cu (–Mo) deposit.

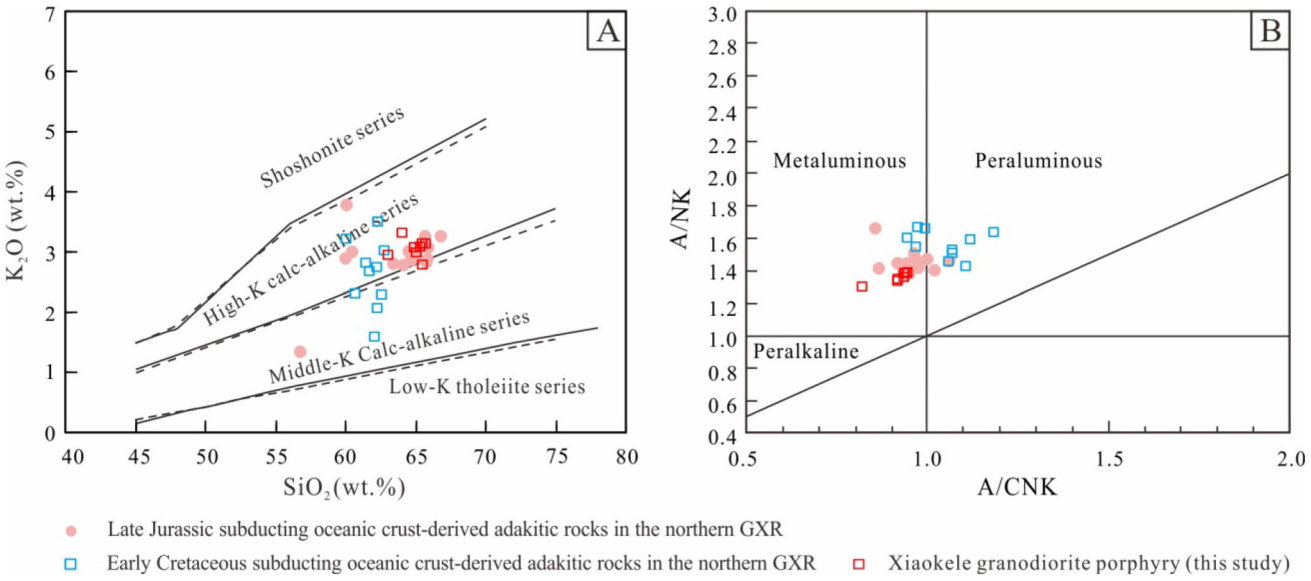

Fig. 5 **A** SiO_2 vs. K_2O plot and **B** A/CNK vs. A/NK plot for the granodiorite porphyry from the Xiaokele deposit. Data for the Late Jurassic subducting oceanic crust-derived adakitic rocks in the northern GXR are from Deng et al. (2019a) and Deng et al. (2019b), whereas data for the Early Cretaceous subducting oceanic crust-derived adakitic rocks in the northern GXR are from Xu et al. (2020)

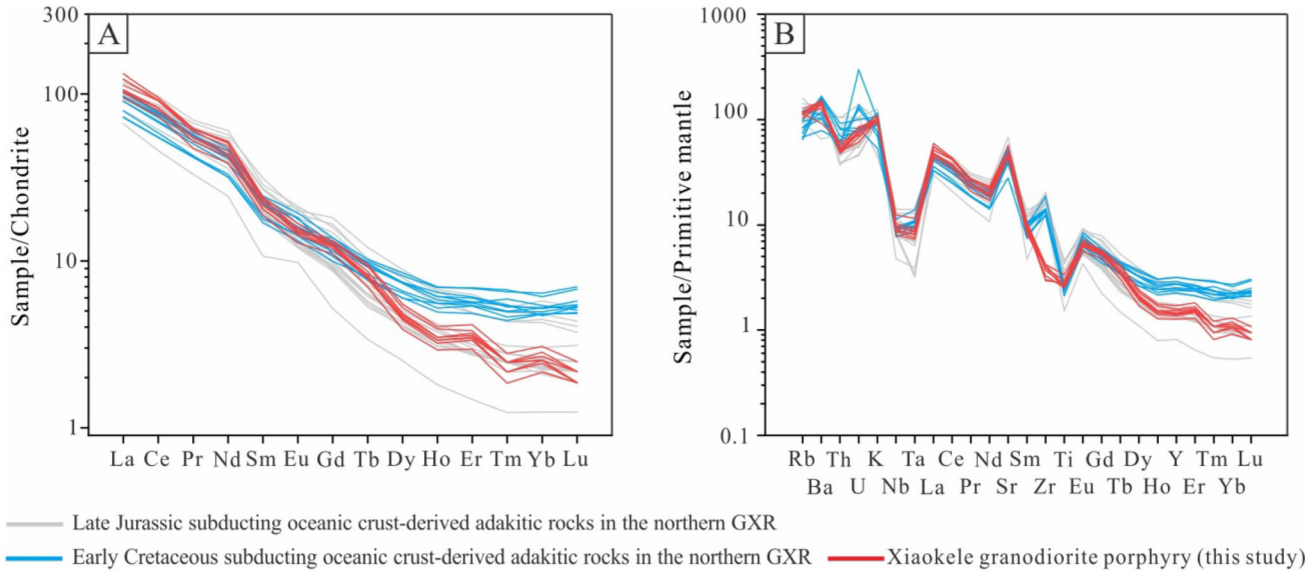

Fig. 6 **A** Chondrite-normalized REE patterns and **B** primitive mantle-normalized spider diagrams for the granodiorite porphyry from the Xiaokele deposit. The chondrite values are from Boynton (1984), the primitive mantle values are from Sun and McDonough (1989). Data for the Late Jurassic-Early Cretaceous subducting oceanic crust-derived adakitic rocks in the northern GXR are from the same data sources as in Fig. 5

6.2 Petrogenesis of the Xiaokele ore-bearing granodiorite porphyry

The Xiaokele granodiorite porphyries have high SiO_2 (63.01–65.70 wt.%, > 56.0 wt.%), Al_2O_3 (15.83–16.43 wt.%, > 15.0 wt.%), Sr (918–1196 ppm, > 400 ppm), Sr/Y ratios (141–160), and low Y (5.76–7.76 ppm, < 18 ppm) and Yb (0.45–0.64 ppm, < 1.9 ppm), as well as weakly negative Eu anomalies ($Eu/Eu^* = 0.80–0.91$), showing a geochemical affinity to adakites (Defant and Drummond 1990; Kay and Kay 1993; Kay et al. 1993). All the Xiaokele granodiorite porphyry samples plot in the typical adakitic rocks field in the Yb_N versus $(La/Yb)_N$ and Y versus Sr/Y geochemical classification diagrams (Fig. 8A, B). Adakitic magmas can be produced by partial melting of subducted oceanic slabs (Defant and Drummond 1990; Martin et al. 2005), assimilation–fractional crystallization (AFC) processes of

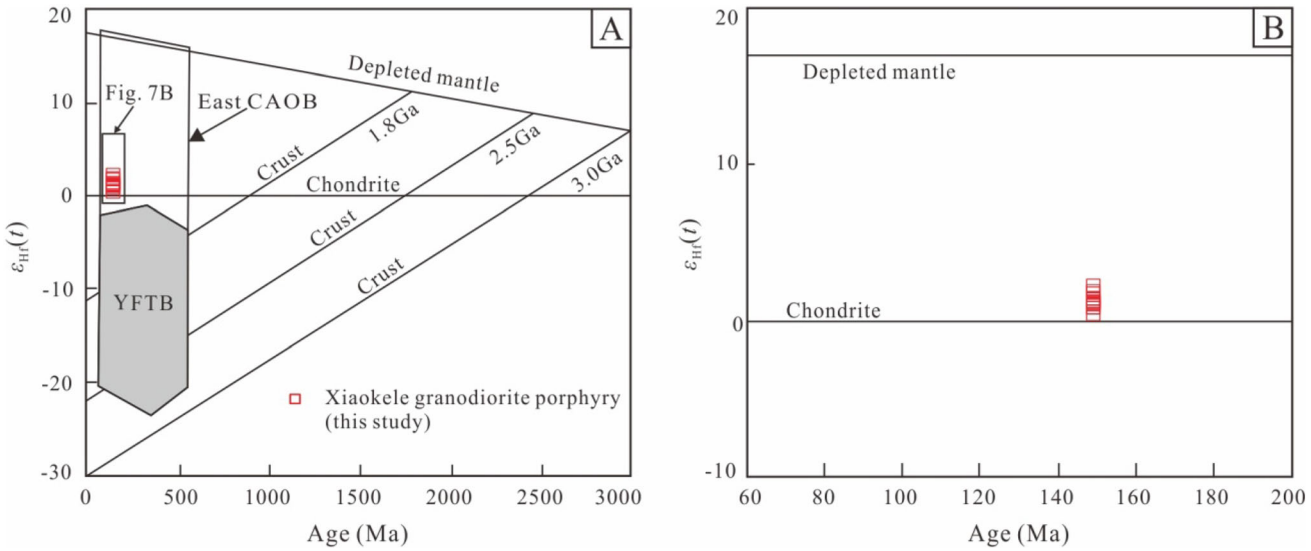

Fig. 7 **A** Plots of zircon U–Pb ages vs. $\varepsilon_{Hf}(t)$ values for the granodiorite porphyry from the Xiaokele deposit. YFTB = Yanshan Fold-and-Thrust Belt (Yang et al. 2006). **B** Close-up view of the distribution of samples in Fig. 7A

basaltic magmas (Castillo et al. 1999; Macpherson et al. 2006), mixing between crustal and mantle magma (Guo et al. 2007; Richards and Kerrich 2007; Streck et al. 2007), partial melting thickened mafic lower continental crust (LCC) (Atherton and Petford 1993; Condie 2005; Deng et al. 2018), partial melting of subducted continental crust (Wang et al. 2008, 2010), or partial melting of the delaminated LCC (Kay and Kay 1993; Xu et al. 2002; Hou et al. 2007; Kadioglu and Dilek 2010).

The negligible Eu anomalies indicate little or no plagioclase fractionation (Macpherson et al. 2006). The high-pressure fractional crystallization (HPFC) of a garnet-bearing assemblage from parental basaltic melts will commonly exhibit a positive relationship of SiO_2 with either Dy/Yb or Sr/Y ratios (Macpherson et al. 2006), but the adakitic rocks show no such correlations (Fig. 8C, D). Hornblende fractionation would result in high Sr/Y ratios, but there are no correlations between SiO_2 and Sr/Y (Fig. 8D). We propose that partial melting played a dominant role in magma formation based on a similar compositional trend to the partial melting process (Fig. 8E, F). In addition, there is no large volume of coeval mafic rocks in the Xiaokele area, excluding the possibility for the generation of adakitic magma through AFC processes (Deng et al. 2019a; Feng et al. 2020a). Mixing between crustal and mantle magma would result in magmatic rocks with a wide range of geochemical characteristics, but the granodiorite porphyries have relatively homogenous whole-rock geochemical and zircon Hf isotopic compositions. Moreover, mafic microgranular enclaves (MMEs) are absent in the granodiorite porphyries, further indicating that they were not derived from mixed magma.

Partial melting of delaminated mafic LCC would produce adakites with high MgO, Cr, and Ni contents and $Mg^{\#}$ values as a result of reaction with surrounding mantle peridotites (Xu et al. 2002; Huang et al. 2008). However, this is inconsistent with the low Cr (13.87–43.73 ppm) and Ni (9.02–16.10 ppm) contents of the Xiaokele granodiorite porphyries. In addition, the delamination of LCC is usually confined to the regions which are undergoing crustal extension (Wang et al. 2007). Delamination of LCC is unlikely to occur because of simultaneous thrust-nappe structure in the Mohe Basin (Chang et al. 2007) and strong deformation of Late Mesozoic igneous rocks in the Erguna Block (Tang et al. 2015). All the evidence suggests that the GXR was controlled by a compressive regime during the Late Jurassic–early Early Cretaceous. Accordingly, it seems unlikely that the Xiaokele granodiorite porphyries were derived from the partial melting of the delaminated LCC.

The Xiaokele granodiorite porphyry samples are sodic with Na_2O = 4.90–5.54 wt.% and K_2O = 2.79–3.32 wt.%. Their K_2O/Na_2O ratios vary from 0.53 to 0.65 (average = 0.60). In the Al_2O_3 vs. K_2O/Na_2O diagram, they plot in the area of oceanic slab-derived adakites for their low K_2O/Na_2O ratios and high Al_2O_3 contents (Fig. 9A), which are different from typical lower-crust-derived adakites with high K_2O/Na_2O ratios (Xiao and Clemens 2007). The Xiaokele granodiorite porphyry samples display low $(La/Yb)_N$ (average = 43.2) but high variable Sr/Y (141–160; average = 152), which are also comparable to adakites related to slab melting in subduction zones (Fig. 9B). In addition, adakites derived from subduction zones can be classified into two significantly different groups based on SiO_2 contents (Martin et al. 2005). The high-SiO_2 (HSA;

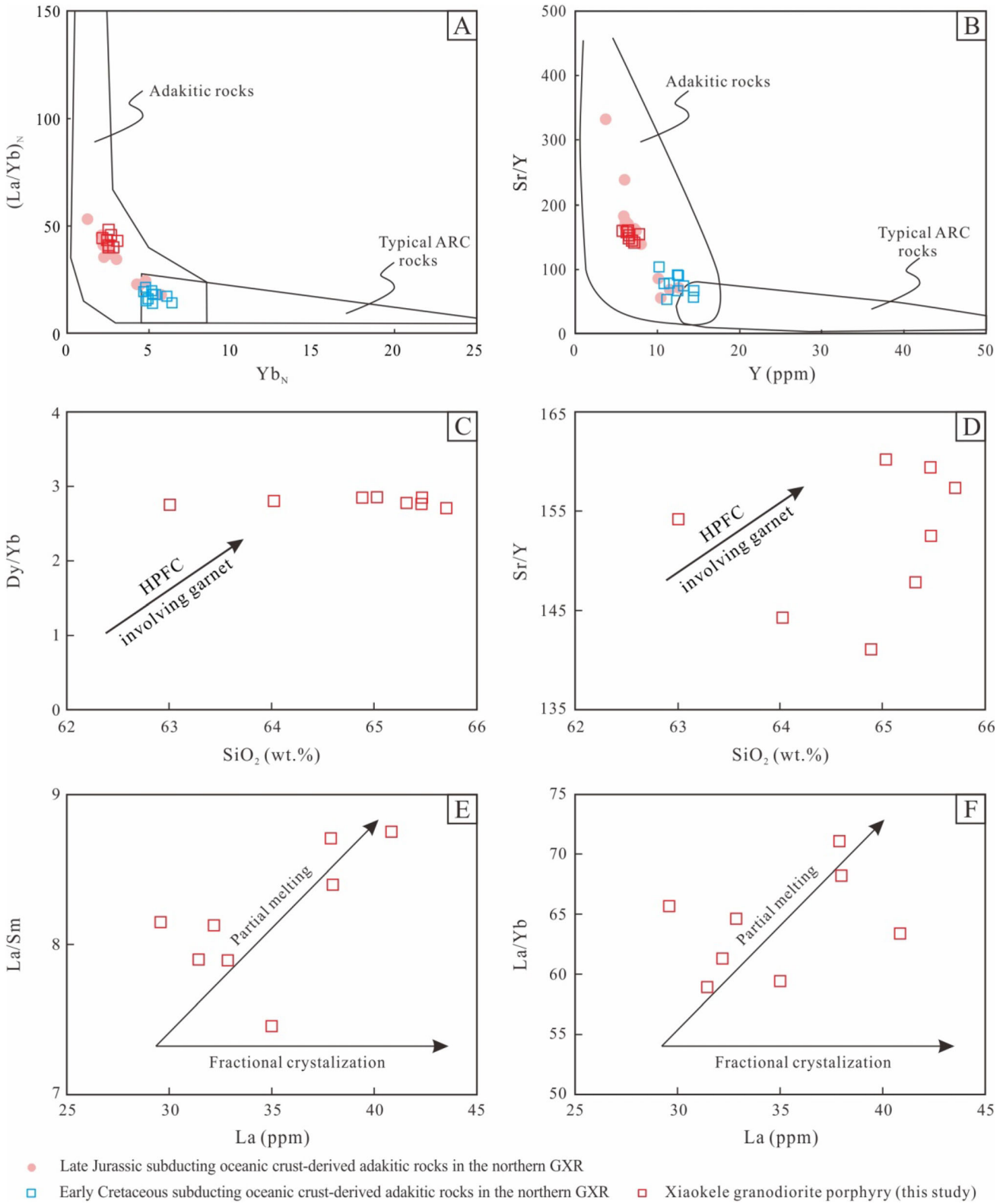

Fig. 8 **A** Yb_N vs. $(La/Yb)_N$ (after Martin 1986), **B** Y vs. Sr/Y (after Defant and Drummond 1990), **C** SiO_2 vs. Dy/Yb, **D** SiO_2 vs. Sr/Y, **E** La vs. La/Sm, and **F** La versus La/Yb diagrams for the granodiorite porphyry from the Xiaokele deposit. Data for the Late Jurassic-Early Cretaceous subducting oceanic crust-derived adakitic rocks in the northern GXR are from the same data sources as in Fig. 5

$SiO_2 > 60\%$, MgO = 0.5–4 wt.%) adakites formed through subducted basaltic slab-melts that reacted with peridotites during ascent through the mantle wedge. The low-SiO_2 (LSA; $SiO_2 < 60\%$, MgO = 4–9 wt.%) adakites formed through melts of peridotitic mantle wedge that was modified by reaction with felsic slab-melts (Martin et al. 2005). In the discrimination diagrams for HSA and LSA (Fig. 9C-F), the Xiaokele granodiorite porphyry samples are mainly distributed in the HSA field, indicating an interaction between slab-derived melts and mantle peridotites. Regionally, the Late Jurassic-Early Cretaceous adakitic rocks in the northern GXR (Fig. 8A, B) show geochemical characteristics similar to the Xiaokele granodiorite porphyry (Figs. 5, 6), they were suggested to be produced by partial melting of an oceanic slab (Fig. 9; Deng et al. 2019a, b; Xu et al. 2020).

However, the lower zircon $\varepsilon_{Hf}(t)$ values of the Xiaokele granodiorite porphyries relative to the depleted mantle (Fig. 7) suggest that ancient crustal materials were involved in the genesis of the Xiaokele granodiorite porphyries besides the subducted MORB. These crustal materials may be continental crust materials added through crustal contamination or magma mixing, or the subducted marine sediments added in the source during slab melting (Deng et al. 2019c; Qi et al. 2020). The model of magma mixing is not favored as mentioned above. No xenocrystic zircons were found in the Xiaokele granodiorite porphyry samples, suggesting that negligible crustal contamination occurred during magma ascent. Thus the ancient crustal materials added in the source of the Xiaokele granodiorite porphyries are most likely the subducted marine sediments. The marine sediments generally display high Sr and Nd contents, and highly enriched radiogenic isotopic compositions, thus the Sr–Nd isotopic compositions of adakites derived from oceanic crust can be enriched through the addition of a small number of marine sediments in the source (Elliott et al. 1997; Wang et al. 2013). The Xiaokele granodiorite porphyries have slightly enriched Sr–Nd isotopic compositions [$(^{87}Sr/^{86}Sr)_i = 0.7055–0.7057$, $\varepsilon_{Nd}(t) = -1.17 -- 0.27$] (Deng et al. 2019a), suggesting the involvement of marine sediments in the source. Sr–Nd isotopic data of the Xiaokele granodiorite porphyries and Jurassic granitoids in the GXR appear the trend towards the EMII end member, and similar to the typical trend of marine sediments (Hofmann 2003), also reflecting the significant role of marine sediments in their source (Fig. 10). Moreover, marine sediments generally display high Th contents (Hawkesworth et al. 1997), thus Th contents could be increased by the involvement of marine sediments in the magma source (Woodhead et al. 2001). In the Ba/La versus Th/Yb diagram (Fig. 11), the Xiaokele granodiorite porphyries display trends characteristic of sediments or sediment melts, further indicating the involvement of marine sediments.

Therefore, based on the above discussion, we suggest that the Xiaokele granodiorite porphyries were produced by partial melting of a subducted oceanic slab, with the involvement of marine sediments in the source, followed by interaction with the mantle peridotites during ascent through the mantle wedge.

6.3 Implications for regional tectonic setting

The generation of Late Mesozoic magmatism in the GXR has been debated to be related to the Paleo-Pacific (Zhang et al. 2010; Hu et al. 2014; Liu et al. 2014; Shu et al. 2016) or the Mongol–Okhotsk tectonic regime (Ying et al. 2010; Xu et al. 2013; Tang et al. 2016; Chen et al. 2017b; Deng et al. 2019b). However, the Late Jurassic–early Early Cretaceous (150–130 Ma) porphyry Cu–Mo deposits in NE China are spatially confined to the western part of the Songliao Basin, and concentrated in the GXR and western part of North China Craton, but not distributed in the eastern part (Chen et al. 2017b; Zhang and Li 2017). This scenario suggests a genetic relation to the evolution of the Mongol–Okhotsk Ocean rather than the Paleo-Pacific Ocean (Chen et al. 2017b). However, the subduction history of the Mongol–Okhotsk Ocean has not been well constrained, some researchers propose that the Erguna Block was in a post-orogenic extensional setting related to the closure of the Mongol-Okhotsk Ocean during Late Jurassic–Early Cretaceous (Mao et al. 2013; Li et al. 2014; Han et al. 2020), while other researchers conclude that the southwards subduction of the Mongol–Okhotsk Ocean continues to occur during Late Jurassic–Early Cretaceous (Zhang 2014; Deng et al. 2019a, 2019b; Zhang et al. 2019). This is because the final closing time of the Mongol–Okhotsk Ocean is still controversial, the Mongol–Okhotsk Ocean might have finally closed during the Middle Jurassic (Sun et al. 2013; Li et al. 2018) or the Late Jurassic–Early Cretaceous (Zonenshain and Kuzmin 1997; Metelkin et al. 2010; Pei et al. 2011; Yang et al. 2015).

Extensive paleomagnetic studies have shown that the Mongol–Okhotsk Ocean was still thousands of kilometers wide in the Late Jurassic and finally closed in the Early Cretaceous (Cogné et al. 2005; Pei et al. 2011). Zhang et al. (2019) proposed that the middle sector of the Mongol–Okhotsk Ocean did not close until 110 Ma based on a compilation of updated paleomagnetic data in support of the latest Early Cretaceous final ocean closure. Therefore, these multiple lines of evidence strongly suggest that the Mongol–Okhotsk oceanic slab may have maintained southward subduction in the Late Jurassic. This conclusion can also be supported by studies of petrogeochemistry on Late Jurassic porphyry deposits in the northern GXR. The

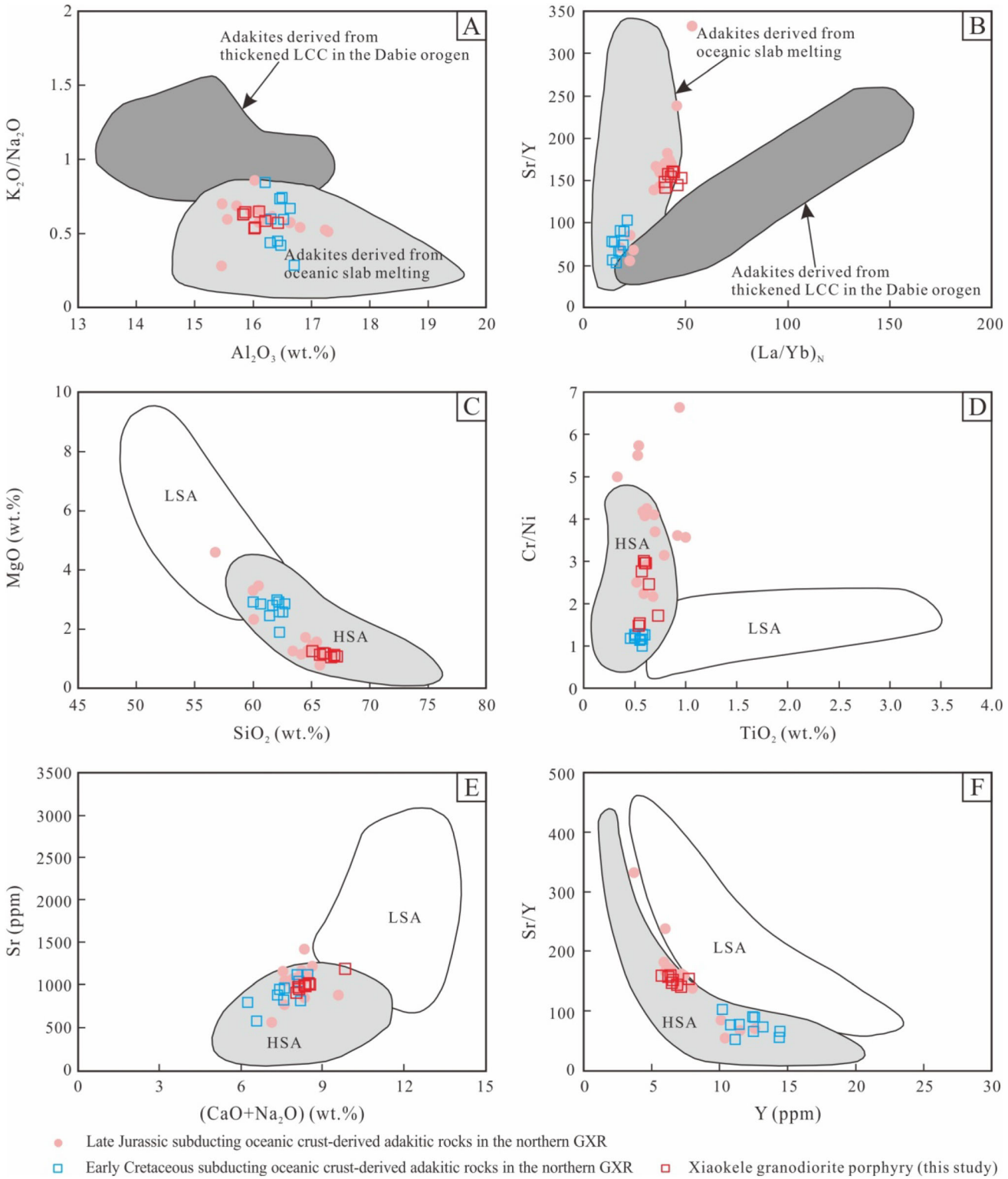

Fig. 9 **A** Al_2O_3 vs. K_2O/Na_2O, **B** $(La/Yb)_N$ vs. Sr/Y, **C** SiO_2 vs. MgO, **D** TiO_2 vs. Cr/Ni, **E** $(CaO + Na_2O)$ vs. Sr, and **F** Y vs. Sr/Y diagrams for the granodiorite porphyry from the Xiaokele deposit. Figure 9**C**, **F** is after Martin et al. (2005). The field of adakites derived from the thickened lower continental crust (LCC) in the Dabie orogeny is from Wang et al. (2007), He et al. (2010), and Liu et al. (2010b); the field of adakites derived from oceanic slab melting is from Kamei et al. (2009). Data for the Late Jurassic-Early Cretaceous subducting oceanic crust-derived adakitic rocks in the northern GXR are from the same data sources as in Fig. 5. Abbreviations: HSA = high-SiO_2 adakitic rocks; LSA = low-SiO_2 adakitic rocks

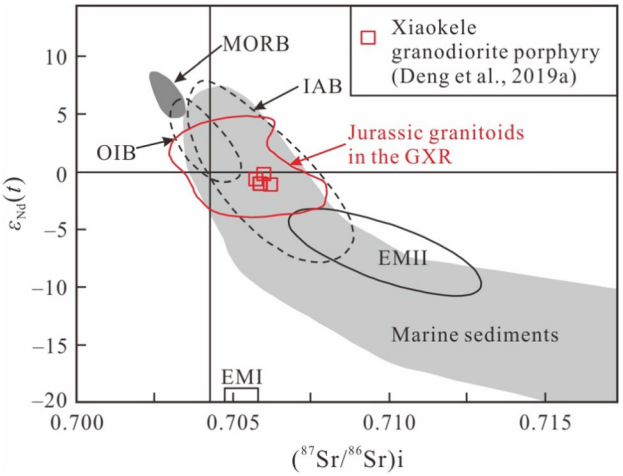

Fig. 10 Sr–Nd isotopic compositions of the granodiorite porphyry from the Xiaokele deposit. Sr–Nd isotopic data source: the fields for MORB, OIB, and IAB are from Vervoort et al. (1999); the field for marine sediments is from Hofmann (2003); EMI and EMII represent two types of mantle end-members (Hou et al. 2011); the Xiaokele granodiorite porphyries are from Deng et al. (2019a); the Jurassic granitoids in the Great Xing'an Range is from Wu et al. (2002), Chen et al. (2011), Hu et al. (2016), and Deng et al. (2019b). Abbreviations: MORB = mid-ocean ridge basalt; OIB = ocean island basalt; IAB = island arc basalt

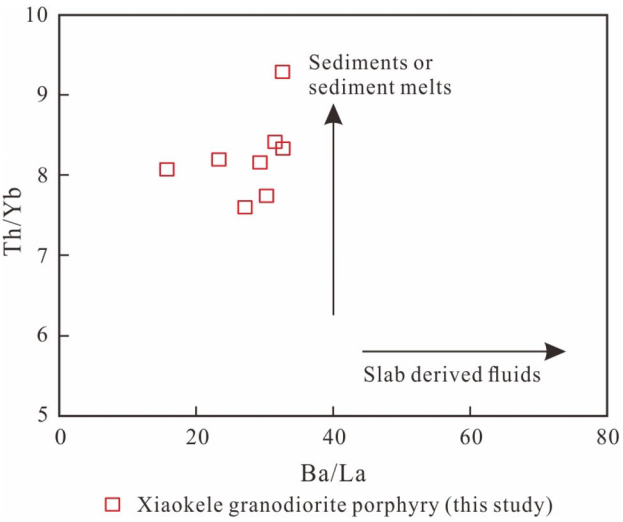

Fig. 11 Ba/La versus Th/Yb diagram (after Woodhead et al. 2001) for the granodiorite porphyry from the Xiaokele deposit to distinguish the contribution of subducted sediments in the source

published whole rocks geochemical data for Late Jurassic quartz diorite porphyries associated with Cu (Mo) mineralization in the Fukeshan deposit indicate that they possibly derived from the melting of an oceanic slab, forming in the subduction tectonic setting related to Mongol–Okhotsk oceanic slab tectonic activities (Deng et al. 2019b). Moreover, in this study, Late Jurassic adakitic ore-bearing granodiorite porphyries in the Xiaokele porphyry Cu (–Mo) deposit belong to adakitic rocks, also derived from the partial melting of subducted oceanic crust, such that the Xiaokele deposit is most likely the product of southward subduction of the Mongol–Okhotsk Ocean. Therefore, Late Jurassic porphyry deposits are extremely likely to be related to intermediate-felsic porphyritic intrusions with subduction-related geochemical features and are interpreted to be the product of the southward subduction of the Mongol–Okhotsk oceanic plate (Zhang and Li 2017; Deng et al. 2019a; Guo et al. 2020).

7 Conclusions

(1) LA–ICP–MS zircon U–Pb dating shows that the Xiaokele granodiorite porphyries were emplaced at 148.8 ± 1.1 Ma.

(2) The Xiaokele ore-bearing granodiorite porphyries are adakites produced by partial melting of the subducted oceanic slab, with involvement of marine sediments in the magma source, followed by interaction with the mantle peridotites during ascent through the mantle wedge.

(3) The Xiaokele granodiorite porphyries were the product of the southward subduction of the Mongol–Okhotsk Ocean.

Supplementary Information The online version contains supplementary material available at https://doi.org/10.1007/s11631-021-00485-z.

Acknowledgements We would like to thank the staff members of the Qiqihaer Institute of Geological Exploration, Heilongjiang, China for sample collection. This research was funded by the National Natural Science Foundation of China (No. 41272093), National Key R&D Program of China (No. 2017YFC0601304), Natural Science Foundation of Jilin Province (No. 20180101089JC), Key Projects of Science and Technology Development Plan of Jilin Province (No. 20100445), Self-determined Foundation of Key Laboratory of Mineral Resources Evaluation in Northeast Asia, Ministry of Natural Resources (No. DBY-ZZ-19-04), and Heilongjiang Research Project of Land and Resources (No. 201605 and 201704).

Declarations

Conflict of interest We declare no conflicts of interest in this study.

References

Andersen T (2002) Correction of common lead in U-Pb analyses that do not report ^{204}Pb. Chem Geol 192:59–79

Atherton MP, Petford N (1993) Generation of sodium-rich magmas from newly underplated basaltic crust. Nature 362:144–146

Boynton WV (1984) Cosmochemistry of the rare earth elements: meteorite studies. In: Henserson P (ed) Rare earth element geochemistry. Elsevier, Amsterdam, pp 63–114

Castillo PR, Janney PE, Solidum RU (1999) Petrology and geochemistry of Camiguin Island, southern Philippines: insights to the source of adakites and other lavas in a complex arc setting. Contrib Miner Petrol 134:33–51

Chang LH, Wang XY, Wang XZ, Zhao BX, Liang HJ (2007) Characteristics and evolution of thrust nappe structure in the Mohe area, Daxing'anling. J Jilin Univ (Earth Sci Ed) 37: 11–15 ((sup) (in Chinese with English Abstract))

Chen YJ, Santosh M (2014) Triassic tectonics and mineral systems in Qinling Orogen. China Geol J 49:338–358

Chen ZG, Zhang LC, Wan B, Wu HY, Cleven N (2011) Geochronology and geochemistry of the Wunugetushan porphyry Cu–Mo deposit in NE china, and their geological significance. Ore Geol Rev 43:92–105

Chen YJ, Zhang C, Li N, Yang YF, Deng K (2012) Geology of the Mo deposits in Northeast China. J Jilin Univ (Earth Sci Ed) 42(5): 1223–1254 (in Chinese with English abstract)

Chen YJ, Wang P, Li N, Yang YF, Pirajno F (2017a) The collision–type porphyry Mo deposits in Dabie Shan. China Ore Geol Rev 81:405–430

Chen YJ, Zhang C, Wang P, Pirajno F, Li N (2017b) The Mo deposits of Northeast China: a powerful indicator of tectonic settings and associated evolutionary trends. Ore Geol Rev 81:602–640

Cogné JP, Kravchinsky VA, Halim N, Hankard F (2005) Late Jurassic-Early Cretaceous closure of the Mongol-Okhotsk Ocean demonstrated by new Mesozoic palaeomagnetic results from the Trans-Baikal area (SE Siberia). Geophys J Int 163:813–832

Condie KC (2005) TTGs and adakites: are they both slab melts? Lithos 80:33–44

Defant MJ, Drummond MS (1990) Derivation of some modern arc magmas by melting of young subducted lithosphere. Nature 347:662–665

Deng CZ, Sun GY, Sun DY, Huang H, Zhang JF, Gou J (2018) Origin of C type adakite magmas in the NE Xing'an block, NE China and tectonic implication. Acta Geochim 37:281–294

Deng CZ, Sun DY, Han JS, Li GH, Feng YZ, Xiao B, Li RC, Shi HL, Xu GZ, Yang DG (2019a) Ages and petrogenesis of the Late Mesozoic igneous rocks associated with the Xiaokele porphyry Cu-Mo deposit, NE China and their geodynamic implications. Ore Geol Rev 107:417–433

Deng CZ, Sun DY, Han JS, Chen HY, Li GH, Xiao B, Li RC, Feng YZ, Li CL, Lu S (2019b) Late-stage southwards subduction of the Mongol-Okhotsk oceanic slab and implications for porphyry Cu-Mo mineralization: constraints from igneous rocks associated with the Fukeshan deposit, NE China. Lithos 326–327:341–357

Deng JH, Yang XY, Qi HS, Zhang ZF, Mastoi AS, Berador AEG, Sun WD (2019c) Early Cretaceous adakite from the Atlas porphyry Cu-Au deposit in Cebu Island, Central Philippines: partial melting of subducted oceanic crust. Ore Geol Rev 110:102937

Elliott T, Plank T, Zindler A, White W, Bourdon B (1997) Element transport from slab to volcanic front at the Mariana arc. J Geophys Res-Solid Earth 102:14991–15019

Feng YZ, Chen HY, Xiao B, Li RC, Deng CZ, Han JS, Li GH, Shi HL, Lai CK (2020a) Late Mesozoic magmatism at Xiaokelehe Cu–Mo deposit in Great Xing'an Range, NE China: Geodynamic and metallogenic implications. Lithos 374–375:105713

Feng YZ, Deng CZ, Chen HY, Li GH, Xiao B, Li RC, Shi HL (2020b) Re-Os isotopic dating of sulfides from the Xiaokelehe Cu-Mo deposit in the Northern part of the Great Xing'an Range, NE China, and its geological implications. Geotecton Metallog 3:465–475

Ge WC, Wu FY, Zhou CY, Rahman AA (2005) Emplacement age of the Tahe granite and its constraints on the tectonic nature of the Erguna block in the northern part of the Da Hinggan Range. Chin Sci Bull 50(18):2097–2105

Gou J, Sun DY, Ren YS, Hou XG, Yang DG (2017) Geochemical and Hf isotopic compositions of Late Triassic-Early Jurassic intrusions of the Erguna Block, Northeast China: petrogenesis and tectonic implications. Int Geol Rev 59:347–367

Guo F, Nakamuru E, Fan WM, Kobayoshi K, Li CW (2007) Generation of Palaeocene adakitic andesites by magma mixing; Yanji Area, NE China. J Petrol 48:661–692

Guo XG, Li JW, Zhang DH, Xue F, Xian HB, Wang SJ, Jiao TL (2020) Petrogenesis and tectonic setting of igneous rocks from the Dongbulage porphyry Mo deposit, Great Hinggan Range, NE China: Constraints from geology, geochronology, and isotope geochemistry. Ore Geol Rev 120:103326

Han R, Qin KZ, Su SQ, Groves DI, Zhao C, Hui KX, Meng ZJ (2020) An Early Cretaceous Ag-Pb-Zn mineralization at Halasheng in the South Erguna Block, NE China: Constraints from U-Pb and Rb-Sr geochronology, geochemistry and Sr-Nd-Hf isotopes. Ore Geol Rev 122:103526

Hawkesworth CJ, Turner SP, McDermott F, Peate DW, van Calsteren P (1997) U-Th isotopes in arc magmas: implications for element transfer from the subducted crust. Science 276:551–555

He YS, Li SG, Hoefs J, Huang F, Liu S (2010) Partial melts from thick lower continental crust: geochemical characterization and identification. Geochim Cosmochim Ac 74: A392

Hofmann AW (2003) Sampling mantle heterogeneity through oceanic basalts: isotopes and trace elements. In: Carlson RW (ed) The Mantle and core. Treatise on geochemistry. Elservier Pergamon, Oxford, pp 61–101

Hollings P, Cooke DR, Waters PJ, Cousens B (2011) Igneous geochemistry of mineralized rocks of the Baguio district, philippines: implications for tectonic evolution and the genesis of porphyry-style mineralization. Econ Geol 106:1317–1333

Hoskin PWO (2005) Trace-element composition of hydrothermal zircon and the alteration of Hadean zircon from the Jack Hills. Aust Geochim Cosmochim Acta 69(3):637–648

Hou ZQ, Zaw K, Pan GT, Mo XX, Xu Q, Hu YZ, Li XZ (2007) Sanjiang Tethyan metallogenesis in SW China: tectonic setting, metallogenic epochs and deposit types. Ore Geol Rev 31:48–87

Hou ZQ, Zhang H, Pan X, Yang Z (2011) Porphyry Cu (-Mo-Au) deposits related to melting of thickened mafic lower crust: examples from the eastern Tethyan metallogenic domain. Ore Geol Rev 39:21–45

Hu XL, Yao SZ, He MC, Ding ZJ, Cui YB, Shen J, Chen B, Zhu BP (2014) Geochemistry, U-Pb geochronology and Hf isotope studies of the Daheishan porphyry Mo deposit in Heilongjiang Province, NE China. Res Geol 64:102–116

Hu XL, Ding ZJ, Yao SZ, He MC, Shen J, Zhu BP, Chen B (2016) Geochronology and Sr–Nd–Hf isotopes of the Mesozoic granitoids from the Great Xing'an and Lesser Xing'an ranges: implications for petrogenesis and tectonic evolution in NE China. Geol J 51(1):1–20

Huang F, Li S, Dong F, He Y, Chen F (2008) High-Mg adakitic rocks in the Dabie orogen, Central China: implications for foundering mechanism of lower continental crust. Chem Geol 255:1–13

IMBGMR (Inner Mongolian Bureau of Geology and Mineral Resources) (1991) Regional Geology of Inner Mongolia. Geological Publishing House, Beijing, p 1–725 (in Chinese with English abstract)

IMBGMR (Inner Mongolian Bureau of Geology Mineral Resources) (1996) Lithostratigraphy of Inner Mongolia. China University of Geosciences Press, Wuhan, p 1–342 (in Chinese with English Abstract)

Jahn BM, Wu FY, Chen B (2000) Granitoids of the Central Asian Orogenic Belt and continental growth in the Phanerozoic. Earth Environ Sci Trans R Soc 91:181–193

Jahn BM, Windley B, Natal'in B, Dobretsov N (2004) Phanerozoic continental growth in Central Asia. J Asian Earth Sci 23(5):599–603

Kadioglu YK, Dilek Y (2010) Structure and geochemistry of the adakitic Horoz granitoid, Bolkar Mountains, south-central Turkey, and its tectonomagmatic evolution. Int Geol Rev 52:505–535

Kamei A, Miyake Y, Owada M, Kimura JI (2009) A pseudo adakite derived from partial melting of tonalitic to granodioritic crust, Kyushu, southwest Japan arc. Lithos 112:615–625

Kay RW, Kay SM (1993) Delamination and delamination magmatism. Tectonophys 219(219):177–189

Kay SM, Ramos VA, Marquez M (1993) Evidence in Cerro Pampa volcanic rocks of slab melting prior to ridge trench collision in southern South America. J Geol 101:703–714

Li ZZ, Qin KZ, Li GM, Ishihara S, Jin LY, Song GX, Meng ZJ (2014) Formation of the giant Chalukou porphyry Mo deposit in northern Great Xing'an Range, NE China: partial melting of the juvenile lower crust in intra-plate extensional enrironment. Lithos 202–203:138–156

Li Y, Xu WL, Tang J, Pei FP, Wang F, Sun CY (2018) Geochronology and geochemistry of Mesozoic intrusive rocks in the Xing'an Massif of NE China: implications for the evolution and spatial extent of the Mongol-Okhotsk tectonic regime. Lithos 304–307:57–73

Liu YS, Hu ZC, Gao S et al (2008) In situ analysis of major and trace elements of anhydrous minerals by LA-ICP-MS without applying an internal standard. Chem Geol 257:34–43

Liu SA, Li SG, He YS, Huang F (2010a) Geochemical contrasts between early Cretaceous ore-bearing and ore-barren high-Mg adakites in central-eastern China: implications for petrogenesis and Cu–Au mineralization. Geochim Cosmochim Acta 74:7160–7178

Liu YS, Hu ZC, Zong KQ, Gao CG, Gao S, Xu J, Chen HH (2010b) Reappraisement and refinement of zircon U-Pb isotope and trace element analyses by LA-ICP-MS. Chin Sci Bull 55(15):1535–1546

Liu J, Mao JW, Wu G, Luo DF, Hu YQ (2014) Zircon U-Pb and molybdenite Re–Os dating of the Chalukou porphyry Mo deposit in the northern Great Xing'an Range, China and its geological significance. J Asian Earth Sci 79:696–709

Liu YJ, Li WM, Feng ZQ, Wen QB, Neubauer F, Liang CY (2017) A review of the Paleozoic tectonics in the eastern part of Central Asian Orogenic Belt. Gondwana Res 43:123–148

Ludwig KR (2003) User's Manual for Isoplot/Ex v30: A Geochronology Toolkit for Microsoft Excel. Berkeley Geochronological Center Spec Publ 4:25–31

Macpherson CG, Dreher ST, Thirlwall MF (2006) Adakites without slab melting: high pressure differentiation of island arc magma, Mindanao, the Philippines. Earth Planet Sci Lett 243:581–593

Mao JW, Zhou ZH, Wu G, Jiang SH, Liu CL, Li HM, Ouyang HG, Liu J (2013) Metallogenic regularity and minerogenetic series of ore deposits in Inner Mongolia and adjacent areas. Miner Dep 32(4):715–729 (in Chinese with English abstract)

Martin H (1986) Effect of steeper Archean geothermal gradient on geochemistry of subduction-zone magmas. Geology 14:753–756

Martin H, Smithies RH, Rapp R, Moyen JF, Champion D (2005) An overview of adakite, tonalite-trondhjemite-granodiorite (TTG), and sanukitoid: relationships and some implications for crustal evolution. Lithos 79:1–24

Metelkin DV, Vernikovsky VA, Kazansky AY, Wingate MTD (2010) Late Mesozoic tectonics of Central Asia based on paleomagnetic evidence. Gondwana Res 18:400–419

Miao LC, Fan WM, Zhang FQ, Liu DY, Jian P, Shi GH, Tao H, Shi YR (2004) Zircon SHRIMP geochronology of the Xinkailing-Kele complex in the northwestern Lesser Xing'an Range, and its geological implications. Chin Sci Bull 49:201–209

Mungall JE (2002) Roasting the mantle: slab melting and the genesis of major Au and Au-rich Cu deposits. Geology 30:915–918

Oyarzún R, Márquez A, Lillo J, López I, Rivera S (2001) Giant vs small porphyry copper deposits of Cenozoic age in northern Chile: adakitic vs normal calc-alkaline magmatism. Miner Depos 36:794–798

Pei JL, Sun ZM, Liu J, Liu J, Wang XS, Yang ZY, Zhao Y, Li HB (2011) A paleomagnetic study from the Late Jurassic volcanic (155 Ma), North China: Implications for the width of Mongol-Okhotsk Ocean. Tectonophysics 510(3–4):370–380

Qi HS, Lu SM, Yang XY, Zhao LL, Zhou YZ, Deng JH, Li JS (2020) Genesis of Cretaceous igneous rocks and its related large scale porphyry Cu-Au mineralization in Chating, the Middle-Lower Yangtze River Metallogenic Belt: The geochemical constrains. Ore Geol Rev 127:103793

QIGE (Qiqihaer Institute of Geological Exploration) (2018) The research report on the Metallogenic Regularity and Prospecting Potential of Xiaokele Cu (–Mo) Ore District and Periphery at the Xinlin District, Heilongjiang Province, p 1–185 (in Chinese)

Reich M, Parada MA, Palacios C, Dietrich A, Schultz F, Lehmann B (2003) Adakite-like signature of Late Miocene intrusions at the Los Pelambres giant porphyry copper deposit in the Andes of central Chile: Metallogenic implications. Miner Depos 38:876–885

Richards JP (2011a) High Sr/Y arc magmas and porphyry Cu ± Mo ± Au deposits: just add water. Econ Geol 106:1075–1081

Richards JP (2011b) Magmatic to hydrothermal metal fluxes in convergent and collided margins. Ore Geol Rev 40(1):1–26

Richards JP (2015) The oxidation state, and sulfur and Cu contents of arc magmas: implications for metallogeny. Lithos 233:27–45

Richards JP, Kerrich R (2007) Adakite-like rocks: their diverse origins and questionable role in metallogenesis. Econ Geol 102:537–576

Sajona FG, Maury RC (1998) Association of adakites with gold and copper mineralization in the Philippines. C R Acad Sci Ser IIA 326:27–34

Şengör AMC, Natal'in BA, Burtman VS (1993) Evolution of the Altaid tectonic collage and Palaeozoic crustal growth in Eurasia. Nature 364: 299–307

Shen P, Hattori K, Pan H, Jackson S, Seitmuratova E (2015) Oxidation condition and metal fertility of granitic magmas: zircon trace-element data from porphyry Cu deposits in the Central Asian Orogenic Belt. Econ Geol 110:1861–1878

Shu QH, Chang ZS, Lai Y, Zhou YT, Sun Y, Yan C (2016) Regional metallogeny of Mo-bearing deposits in Northeastern China, with New Re-Os dates of porphyry Mo deposits in the Northern Xilamulun District. Econ Geol 111:1783–1798

Sillitoe RH (2010) Porphyry copper systems. Econ Geol 105:3–41

Song BJ, Wang XY, Ma J (2015) Characteristics of geological, genesis and structural background of gold depostis in the north Daxing'anling. Northeast China J Miner Petrol 35(2):15–24

Streck MJ, Leeman WP, Chesley J (2007) High-Mg andesite from Mount Shasta: a product of magma mixing and contamination, not a primitive mantle melt. Geology 35:351–354

Sun SS, McDonough WF (1989) Chemical and isotopic systematics of oceanic basalts: implications for mantle composition and processes. Geol Soc Lond Spec Publ 42(1):313–345

Sun DY, Gou J, Wang TH, Ren YS, Liu YJ, Guo HY, Liu XM, Hu ZC (2013) Geochronological and geochemical constraints on the Erguna massif basement, NE China-subduction history of the Mongol-Okhotsk oceanic crust. Int Geol Rev 55(14):1801–1816

Sun WD, Huang RF, Li H, Hu YB, Zhang CC, Sun SJ, Zhang LP, Ding X, Li CY, Zartman RE (2015) Porphyry deposits and oxidized magmas. Ore Geol Rev 65:97–131

Sun YG, Li BL, Sun FY, Ding QF, Wang BY, Li YJ, Wang K (2020a) Mineralization events in the Xiaokele porphyry Cu (–Mo) deposit, NE China: Evidence from zircon U-Pb and K–feldspar Ar–Ar geochronology and petrochemistry. Res Geol 70(3):254–272

Sun YG, Li BL, Sun FY, Ding QF, Qian Y, Li L, Xu QL, Li YJ (2020b) Geochronology, geochemistry, and Hf isotopic compositions of Early Permian syenogranite and diabase from the northern Great Xing'an Range, NE China: petrogenesis and tectonic implications. Can J Earth Sci 57(12):1478–1491

Tang J, Xu WL, Wang F, Zhao S, Li Y (2015) Geochronology, geochemistry, and deformation history of late Jurassic-Early Cretaceous intrusive rocks in the Erguna Massif, NE China: constraints on the late Mesozoic tectonic evolution of the Mongol-Okhotsk orogenic belt. Tectonophysics 658:91–110

Tang J, Xu WL, Wang F, Zhao S, Wang W (2016) Early Mesozoic southward subduction history of the Mongol-Okhotsk oceanic plate: evidence from geochronology and geochemistry of Early Mesozoic intrusive rocks in the Erguna Massif. NE China Gondwana Res 31:218–240

Vervoort JD, Patchett PJ, Blichert-Toft J, Albarede F (1999) Relationships between Lu-Hf and Sm-Nb isotopic systems in the global sedimentary system. Earth Planet Sci Lett 168:79–99

Wang Q, Wyman DA, Xu J, Jian P, Zhao Z, Li C, Xu W, Ma J, He B (2007) Early Cretaceous adakitic granites in the Northern Dabie Complex, central China: implications for partial melting and delamination of thickened lower crust. Geochim Cosmochim Acta 71(10):2609–2636

Wang Q, Wyman DA, Xu JF, Dong YH, Vasconcelos PM, Pearson N, Wan YS, Dong H, Li CF, Yu YS, Zhu TX, Feng XT, Zhang QY, Zi F, Chu ZY (2008) Eocene melting of subducting continental crust and early uplifting of central Tibet: evidence from central-western Qiangtang high-K calc-alkaline andesites, dacites and rhyolites. Earth Planet Sci Lett 272:158–171

Wang Q, Wyman DA, Li ZX, Sun WD, Chung SL, Vasconcelos PM, Zhang QY, Dong H, Yu YS, Pearson N, Qiu HN, Zhu TX, Feng XT (2010) Eocene north–south trending dikes in central Tibet: new constraints on the timing of east–west extension with implication for early plateau uplift? Earth Planet Sci Lett 298:205–216

Wang FY, Liu SA, Li SG, He YS (2013) Contrasting zircon Hf-O isotopes and trace elements between ore-bearing and ore-barrenadakitic rocks in central-eastern China: implications for genetic relation to Cu-Au mineralization. Lithos 156–159:97–111

Woodhead JD, Hergt JM, Davidson JP, Eggins SM (2001) Hafnium isotope evidence for 'conservative' element mobility during subduction zone processes. Earth Planet Sci Lett 192:331–346

Wu FY, Sun DY, Li HM, Jahn BM, Wilde S (2002) A-type granites in northeastern China: age and geochemical constraints on their petrogenesis. Chem Geol 187:143–173

Wu FY, Yang YH, Xie LW et al (2006) Hf isotopic compositions of the standard zircons and baddeleyites used in U-Pb geochronology. Chem Geol 234(1–2):105–126

Wu FY, Sun DY, Ge WC, Zhang YB, Grant ML, Wilde SA, Jahn BM (2011) Geochronology of the Phanerozoic granitoids in northeastern China. J Asian Earth Sci 41:1–30

Xiao L, Clemens JD (2007) Origin of potassic (C-type) adakite magmas: experimental and field constraints. Lithos 95:399–414

Xu JF, Shinjo R, Defant MJ, Wang QA, Rapp RP (2002) Origin of Mesozoic adakitic intrusive rocks in the Ningzhen area of east China: partial melting of delaminated lower continental crust? Geology 30:1111–1114

Xu WL, Pei FP, Wang F, Meng E, Ji WQ, Yang DB, Wang W (2013) Spatialtemporal relationships of Mesozoic volcanic rocks in NE China: constraints on tectonic overprinting and transformations between multiple tectonic regimes. J Asian Earth Sci 74:167–193

Xu GZ, Deng CZ, Li CL, Lv CL, Yin RS, Ding JS, Yuan MW, Gou J (2020) Petrogenesis of Late Carboniferous A-type granites and Early Cretaceous adakites of the Songnen Block, NE China: implications for the geodynamic evolution of the Paleo-Asian and Paleo-Pacific oceans. Lithos 366–367:105575

Yang JH, Wu FY, Shao JA, Wilde SA, Xie LW, Liu XM (2006) Constraints on the timing of uplift of the Yanshan Fold and Thrust Belt. North China Earth Planet Sci Lett 246:336–352

Yang YT, Guo ZX, Song CC, Li XB, He S (2015) A short-lived but significant Mongol-Okhotsk collisional orogeny in latest Jurassic-earliest Cretaceous. Gondwana Res 28:1096–1116

Ying JF, Zhou XH, Zhang LC, Wang F, Zhang YT (2010) Geochronological and geochemical investigation of the late Mesozoic volcanic rocks from the Northern Great Xing'an Range and their tectonic implications. Int J Earth Sci 99:357–378

Yuan HL, Gao S, Liu XM et al (2004) Accurate U-Pb age and trace element determinations of zircon by laser ablation-inductively coupled plasma-mass spectrometry. Geostand Geoanal Res 28:353–370

Zhang KJ (2014) Genesis of the late mesozoic great xing'an range large igneous province in eastern central Asia: A Mongol-Okhotsk slab window model. Int Geol Rev 56(13):1557–1583

Zhang C, Li N (2017) Geochronology and zircon Hf isotope geochemistry of granites in the giant Chalukou Mo deposit, NE China: implications for tectonic setting. Ore Geol Rev 81:780–793

Zhang JH, Ge WC, Wu FY, Wilde SA, Yang JH, Liu XM (2008) Large-scale early cretaceous volcanic events in the northern great xing'an range, Northeastern China. Lithos 102:138–157

Zhang JH, Gao S, Ge WC, Wu FY, Yang JH, Wilde SA, Li M (2010) Geochronology of the Mesozoic volcanic rocks in the Great Xing'an Range, northeastern China: implications for subduction-induced delamination. Chem Geol 276:144–165

Zhang CC, Sun WD, Wang JT, Zhang LP, Sun SJ, Wu K (2017) Oxygen fugacity and porphyry mineralization: a zircon perspective of Dexing porphyry Cu deposit. China Geochim Cosmochim Acta 206:343–363

Zhang KJ, Yan LL, Ji C (2019) Switch of NE Asia from extension to contraction at the mid-Cretaceous: A tale of the Okhotsk oceanic plateau from initiation by the Perm Anomaly to extrusion in the Mongol-Okhotsk ocean? Earth-Sci Rev 198:102941

Zhou JB, Wilde SA, Zhang XZ, Ren SM, Zheng CQ (2011) Early Paleozoic metamorphic rocks of the Erguna block in the Great Xing'an Range, NE China: Evidence for the timing of magmatic and metamorphic events and their tectonic implications. Tectonophysics 499(1–4):105–117

Zhou JB, Wang B, Wilde SA, Zhao GC, Cao JL, Zheng CQ, Zeng WS (2015) Geochemistry and U-Pb zircon dating of the Toudaoqiao blueschists in the Great Xing'an Range, northeast China, and tectonic implications. J Asian Earth Sci 97:197–210

Zhou JB, Wilde SA, Zhao GC, Han J (2018) Nature and assembly of microcontinental blocks within the Paleo-Asian Ocean. Earth-Sci Rev 186:76–93

Zonenshain LP, Kuzmin MI (1997) Paleogeodynamics, the plate tectonic evolution of the earth. American Geophysical Union, Washington, p 218